Frequency Detectors for CPM Signals

Aldo N.D'Andrea, *Senior Member, IEEE*, Alberto Ginesi, and Umberto Mengali, *Fellow, IEEE*

Abstract—**Frequency tracking loops are used in digital links to control the carrier frequency of the received signals. A basic component in such loops is the frequency difference detector (FDD). This paper concentrates on a class of FDDs for use with binary continuous-phase modulation (CPM). Their derivation is based on two ideas: the maximum-likelihood principle for parameter estimation and Laurent's decomposition of a CPM signal into the sum of linearly modulated components. The proposed FDDs are suitable for digital implementation and their operation is independent of clock recovery.**

Analysis and simulation are employed to investigate tracking operation and acquisition capability of frequency control loops endowed with such FDDs. Numerical examples are provided for modulation schemes of practical interest such as MSK and Gaussian MSK. The loop acquisition range is found to be fairly large, about 0.5-1.0 times the bit rate.

I. Introduction

Carrier frequency compensation is needed in digital receivers to cope with oscillator instabilities and Doppler effects. Although compensation methods depend largely on modulation formats and the specific applications, they all employ some type of frequency difference detector (FDD) to measure the difference between the incoming carrier frequency and a local reference.

Several FDD schemes are available for pulse amplitude modulated (PAM) signals. References [1]-[3] describe FDDs for applications where carrier frequency offsets are limited to a fraction of the symbol rate, as happens with high- and medium-capacity digital microwave radios. With low-capacity systems, instead, frequency offsets as large as the symbol rate are encountered and other FDD structures must be resorted to, either in the form of *balanced quadricorrelators* [4]-[9], or *dual filter detector* [7], [10] or algorithms derived from maximum likelihood (ML) methods [11]-[13].

In summary, design engineers have several tools to accomplish carrier frequency recovery with linear modulations. By contrast, the situation is not so satisfactory with continuous phase modulations (CPMs). Indeed, considering the growing interest for these schemes, it is believed that further efforts in this area are necessary.

Studies on carrier frequency recovery for CPM are quite recent and are centered on burst mode transmissions. Reference [14] investigates a data-aided feedforward method for Gaussian MSK. Its performance is remarkably close to the Cramer-Rao bound but its frequency operation range is on the order of 5% of the bit rate. As such, it seems mostly suitable for tracking operations. Another algorithm, proposed in [15], is envisioned for MSK and has a non data-aided feedforward structure. Although its performance does not attain the Cramer-Rao bound, it can manage frequency offsets larger than the method in [14], say up to 25% of the bit rate.

In this paper we investigate closed-loop frequency estimation methods for the class of binary CPM signals. For simplicity, we restrict ourselves to MSK-type modulations, i.e., those with a modulation index h=0.5. Extensions to other values of h are possible but, for space limitations, are not pursued here. Our approach is based on two separate notions: the ML estimation method, as exploited in [11] for PAM modulations, and Laurent's representation of CPM schemes as superpositions of PAM signals [16]. The proposed algorithms are non-data aided and can handle frequency offsets as large as 50-100% of the bit rate (depending on the modulator frequency response). Also, their performance is independent of symbol timing, which makes them particularly useful for initial acquisitions, when data values and timing are all unknown.

The outline of the paper is as follows. Section II describes the signal model and introduces the basic notations. In section III, Laurent's decomposition is overviewed. Next, in section IV, we discuss ML carrier frequency estimation for CPM. This leads us to a frequency control loop involving an FDD whose structure is described in section V. Section VI gives guidelines to assess acquisition characteristics and tracking performance of the loop. Simulation results are reported in section VII to verify the theory. The issue of the loop digital implementation is also addressed. Finally, in section VIII we draw the conclusions.

II. Signal Model

The complex envelope of an MSK-type signal has the expression [17]:

$$s(t) = \sqrt{\frac{2E_b}{T}}\, e^{j\psi(t)}, \tag{1}$$

$$\psi(t) = \pi \sum_i \alpha_i q(t - iT), \tag{2}$$

where E_b represents the energy per symbol, T is the symbol period, $\{\alpha_i\}$ are independent data symbols taking values ± 1 with equal probability, and $q(t)$ is the *phase pulse* of the modulator, which is related to the *frequency pulse*, $g(t)$, by the relationship

$$q(t) = \int_{-\infty}^{t} g(\tau)\, d\tau. \tag{3}$$

Paper approved by Marc Moeneclay, the Editor for Synchronization of the IEEE Communication Society. Manuscript received: March15, 1994; revised: June 6, 1994; November 23, 1994. This work was supported by the Italian Research Council (CNR), grant no. 94.01416.PF74.

The authors are with the Dipartimento di Ingegneria della Informazione, Università di Pisa, Via Diotisalvi 2, 56126 Pisa, Italy.

IEEE Log Number 9411650.

The function $g(t)$ is time-limited to the interval $(0, LT)$ and satisfies the conditions:

$$g(t) = g(LT - t), \tag{4}$$

$$q(LT) = \frac{1}{2}. \tag{5}$$

In numerical examples illustrated in sections VI-VII we consider three different frequency pulses: rectangular (LREC), raised-cosine (LRC), and Gaussian-MSK (GMSK). They are defined as follows:

$$\text{LREC:} \quad g(t) \triangleq \begin{cases} \dfrac{1}{2LT} & 0 \le t \le LT \\ 0 & \text{otherwise} \end{cases} \tag{6}$$

$$\text{LRC:} \quad g(t) \triangleq \begin{cases} \dfrac{1}{2LT}\left[1 - \cos\dfrac{2\pi t}{LT}\right] & 0 \le t \le LT \\ 0 & \text{otherwise} \end{cases} \tag{7}$$

$$\text{GMSK:} \quad g(t) \triangleq \frac{1}{2T}\left\{Q\left[\beta\left(t - \frac{(L+1)T}{2}\right)\right] - Q\left[\beta\left(t - \frac{(L-1)T}{2}\right)\right]\right\}, \tag{8}$$

with

$$Q(x) \triangleq \frac{1}{\sqrt{2\pi}}\int_x^\infty e^{-t^2/2}dt \quad \text{and} \quad \beta \triangleq \frac{2\pi B}{\sqrt{\ln 2}}. \tag{9}$$

The value of L in (8) is such that, with a good approximation, $g(t)$ is limited to the interval $(0, LT)$. For the particular case with BT=0.25 considered later, the value L=4 is appropriate.

III. PAM Representation of CPM Signals

It is clear from (1)-(2) that $\sigma(t)$ depends on $\{\alpha_i\}$ in a nonlinear fashion. As is known, this fact complicates the analysis of most CPM modulations. On the other hand, it has been shown by P.A.Laurent [16] that a binary CPM signal may be viewed as a superposition of a few PAM components, i.e., of time-functions that depend *linearly* on certain coefficients related to the $\{\alpha_i\}$. Laurent's representation (LR) has previously been exploited in [18]-[19] to develop low-complexity receivers for MSK-type modulations. In the next section we adopt LR to derive carrier frequency estimation algorithms. Here we briefly review LR, assuming a modulation index equal to 0.5.

As indicated in [16], the exponential function in (1) may be written as

$$e^{j\psi(t)} = \sum_{m=0}^{M-1}\sum_i a_{m,i}\, h_m(t - iT), \tag{10}$$

where $M \triangleq 2^{L-1}$ and $h_m(t)$ is given by

$$h_m(t) = c(t - LT)\prod_{i=1}^{L-1} c(t - LT + iT + \gamma_{m,i}LT). \tag{11}$$

In this equation, $c(t)$ is defined as

$$c(t) \triangleq \begin{cases} \cos[\pi q(t)] & 0 \le t \le LT \\ c(-t) & -LT \le t < 0 \\ 0 & \text{else} \end{cases} \tag{12}$$

and $\gamma_{m,i}$ is the i-th digit (0 or 1) in the radix-2 representation of the integer m, i.e.,

$$m = \sum_{i=1}^{L-1}\gamma_{m,i}2^{i-1}. \tag{13}$$

Also, the symbols $a_{m,i}$ are related to the data α_i by

$$a_{m,i} = \exp\left\{j\frac{\pi}{2}\left[\alpha_i + \sum_{k=1}^{L-1}\bar{\gamma}_{m,k}\alpha_{i-k} + \sum_{k=-\infty}^{i-L}\alpha_k\right]\right\} \tag{14}$$

with $\bar{\gamma}_{m,k} \triangleq 1 - \gamma_{m,k}$

Some remarks about the above formulas are of interest:

(i) With *full response* systems (L=1), M is unity and there is only one LR component. With *partial response* schemes (L>1), instead, M may be large and (10) may be awkward to handle. It turns out, however, that the energy associated with $h_m(t)$ decreases with m so that, in most cases, only few LR components need to be retained.

(ii) Moments of the symbols $a_{m,i}$ are needed in the following developments. It can been shown that the first-order moments are zero and that the second-order ones are given by [16]

$$E\{a_{m,i}a_{n,k}^*\} = \begin{cases} 1 & m = n \text{ and } i = k \\ 0 & \text{otherwise} \end{cases} \tag{15}$$

(iii) The functions $h_m(t)$ are time limited in the interval $0 \le t \le D_m T$, where D_m takes values in the range $[1, (L+1)]$.

(iv) Making use of (1), (11) and (15), the power spectral density of (1) is found to be

$$\mathcal{S}_s(f) = \frac{2E_b}{T^2}\sum_{m=0}^{M-1}|H_m(f)|^2. \tag{16}$$

In most cases $\mathcal{S}_s(f)$ has negligible values for $|f| \ge 1/T$ (see [17], chapter 4), so that from (16) we have

$$H_m(f) \cong 0 \quad \text{for} \quad |f| \ge 1/T. \tag{17}$$

IV. ML Frequency Estimation

Transmitting (1) over an AWGN channel results in a received voltage with a complex envelope $r(t)$=$s(t)$+$w(t)$. Here, $w(t)$ is a complex-valued Gaussian white noise process with independent components, each with two-sided spectral density N_0, and $s(t)$ is related to (1) by

$$s(t) = e^{j(2\pi\nu t + \theta)}\sigma(t - \tau). \tag{18}$$

In this equation ν represents the offset of the carrier frequency from its nominal value, while θ and τ are the phase shift and the delay introduced by the channel.

Our task is to find the ML estimate of ν. In doing so, we

model ν as a fixed (but unknown) quantity whereas θ and τ, as well as the information data, are seen as *nuisance* random variables. In particular θ and τ are thought of as totally unknown to the receiver and, accordingly, are modeled as uniformly distributed over the intervals $(0,2\pi)$ and $(0,T)$, respectively.

As a first step, we express (18) in the form

$$s(t;\nu,\theta,\tau,\{a_{m,i}\}) = e^{j(2\pi\nu t+\theta)}\sqrt{\frac{2E_b}{T}}\sum_{m=0}^{M-1}\sum_{i} a_{m,i}h_m(t-iT-\tau), \tag{19}$$

which comes from collecting (1) and (10) and replacing $s(t)$ by $s(t;\nu,\theta,\tau,\{a_{m,i}\})$. Assuming that the channel output is observed over some interval $(0, KT)$, the likelihood function takes the form [20]

$$\Lambda(\tilde{\nu},\tilde{\theta},\tilde{\tau},\{\tilde{a}_{m,i}\}) = \exp\left\{\frac{1}{N_0}\int_0^{KT}\mathrm{Re}\left[r(t)s^*(t;\tilde{\nu},\tilde{\theta},\tilde{\tau},\{\tilde{a}_{m,i}\})\right]dt\right\}, \tag{20}$$

where $\tilde{x}$ denotes *trial value of* x and $\mathrm{Re}[x]$ means *real part of* x. A more convenient form for $\Lambda(\tilde{\nu},\tilde{\theta},\tilde{\tau},\{\tilde{a}_{m,i}\})$ is obtained by writing $s(t;\tilde{\nu},\tilde{\theta},\tilde{\tau},\{\tilde{a}_{m,i}\})$ as in (19) and assuming $K>>1$. Substituting into (20) gives

$$\Lambda(\tilde{\nu},\tilde{\theta},\tilde{\tau},\{\tilde{a}_{m,i}\}) = \exp\left\{\sqrt{\frac{2E_b}{T}}\frac{1}{N_0}\times\mathrm{Re}\left[e^{-j\tilde{\theta}}\sum_{m=0}^{M-1}\sum_{k=0}^{K-1}x_m(kT+\tilde{\tau})\tilde{a}^*_{m,k}\right]\right\}, \tag{21}$$

where $x_m(t)$ is the response to $r(t)e^{j2\pi\nu t}$ of a filter matched to $h_m(t)$:

$$x_m(t) = \int_{-\infty}^{\infty} r(z)e^{-j2\pi\tilde{\nu}z}h_m(t-z)\,dz. \tag{22}$$

Note that, as a consequence of (17), $x_m(t)$ has negligible components outside the interval $|f|\le 1/T$.

To get the ML estimate of ν one must first average (21) over the nuisance parameters, so as to obtain the *marginal* likelihood function $\Lambda(\tilde{\nu})$. Then, the desired estimate of ν is found as the abscissa of the maximum of $\Lambda(\tilde{\nu})$. Unfortunately, this route is difficult and we are compelled to make approximations. In particular we assume a low signal-to-noise ratio, such that the exponential in (21) can be expressed as a power series truncated to the second-order term. In other words, defining

$$X = \sqrt{\frac{2E_b}{T}}\frac{1}{N_0}\mathrm{Re}\left[e^{-j\tilde{\theta}}\sum_{m=0}^{M-1}\sum_{k=0}^{K-1}x_m(kT+\tilde{\tau})\tilde{a}^*_{m,k}\right], \tag{23}$$

we write

$$\Lambda(\tilde{\nu},\tilde{\theta},\tilde{\tau},\{\tilde{a}_{m,i}\}) \cong 1 + X + X^2. \tag{24}$$

It should be pointed out that in most practical cases the signal-to-noise ratio is not so low as to justify this expansion. Actually, the basic reason for using (24) is its mathematical tractability. It is likely that better results may be found making more realistic approximations. More research is needed on this topic.

The expectation of (23) with respect to $\tilde{\theta}$, $\tilde{\tau}$ and $\{\tilde{a}_{m,i}\}$ is now easy to compute. Recalling that $\tilde{\theta}$ and $\tilde{\tau}$ are uniformly distributed and that the symbols $\{\tilde{a}_{m,i}\}$ are uncorrelated (see (15)), after some passages it is found:

$$\Lambda(\tilde{\nu}) \cong \int_0^{KT}\left[\sum_{m=0}^{M-1}|x_m(t)|^2\right]dt, \tag{25}$$

where constants and scaling factors independent of $\tilde{\nu}$ have been removed for convenience. In the next section we propose an algorithm to maximize $\Lambda(\tilde{\nu})$. Before doing so, however, it is interesting to consider the following physical interpretation of (25).

Define

$$\bar{r}(t) \triangleq \begin{cases} r(t) & 0\le t\le KT \\ 0 & \text{else} \end{cases} \tag{26}$$

and denote $\bar{R}(f)$ the Fourier transform of $\bar{r}(t)$. Also, let $\bar{x}_m(t)$ and $\bar{X}_m(f)$ be analogous quantities associated with $x_m(t)$. Assuming KT much longer than the duration of $h_m(t)$, from (22) it can be shown that

$$\bar{X}_m(f) = \bar{R}(f+\tilde{\nu})H_m^*(f). \tag{27}$$

On the other hand (25) may be written as (Parseval's theorem)

$$\Lambda(\tilde{\nu}) \cong \int_0^{KT}\left[\sum_{m=0}^{M-1}|X_m(f)|^2\right]df. \tag{28}$$

Thus, substituting (27) into (28) and bearing in mind (16), we get

$$\Lambda(\tilde{\nu}) \cong \frac{T^2}{2E_b}\int_{-\infty}^{\infty}\mathcal{S}_s(f)\left|\bar{R}(f+\nu)\right|^2 df. \tag{29}$$

Since $|\bar{R}(f)|^2$ represents the spectrum of the observed waveform, this equation says that the maximum of $\Lambda(\tilde{\nu})$ is obtained by shifting the received spectrum so as to get the best match with the transmitted spectrum.

V. Frequency Detection Algorithm

The maximum of $\Lambda(\tilde{\nu})$ is obtained by setting to zero the derivative of $\Lambda(\tilde{\nu})$. This derivative reads

$$\frac{\partial\Lambda(\tilde{\nu})}{\partial\tilde{\nu}} \cong 2\int_0^{KT}\sum_{m=0}^{M-1}\mathrm{Re}\left[x_m(t)\frac{\partial x_m^*(t)}{\partial\tilde{\nu}}\right]dt. \tag{30}$$

On the other hand, from (22) one has:

$$\begin{aligned}\frac{\partial x_m(t)}{\partial\tilde{\nu}} &= -j\int_{-\infty}^{\infty}r(z)e^{-j2\pi\tilde{\nu}z}2\pi z\,h_m(z-t)\,dz \\ &= j\int_{-\infty}^{\infty}r(z)e^{-j2\pi\tilde{\nu}z}[2\pi(t-z)]h_m(z-t)\,dz \\ &\quad - j2\pi t\int_{-\infty}^{\infty}r(z)e^{-j2\pi\tilde{\nu}z}h_m(z-t)\,dz,\end{aligned} \tag{31}$$

or, alternatively,

$$\frac{\partial x_m(t)}{\partial \tilde{\nu}} = jy_m(t) - j2\pi t x_m(t), \tag{32}$$

where $y_m(t)$ is given by

$$y_m(t) = \int_{-\infty}^{\infty} r(z)e^{-j2\pi\tilde{\nu}z}[2\pi(t-z)]h_m(z-t)\,dz, \tag{33}$$

Thus, substituting (32) into (30) yields

$$\frac{\partial \Lambda(\tilde{\nu})}{\partial \tilde{\nu}} = \int_0^{KT} u(t)\,dt, \tag{34}$$

where

$$u(t) = 2\sum_{m=0}^{M-1} \mathrm{Im}\{x_m(t)y_m^*(t)\}, \tag{35}$$

and Im{.} means *imaginary part of.*

The following remarks are of interest:

(i) $y_m(t)$ is the response to $r(t)e^{-j2\pi\tilde{\nu}t}$ of a filter with impulse response

$$h'_m(-t) \triangleq 2\pi t h_m(-t); \tag{36}$$

(ii) the Fourier transform of $h'_m(t)$ is

$$H'_m(f) = -j\frac{dH_m(f)}{df}; \tag{37}$$

(iii) like $x_m(t)$, $y_m(t)$ has negligible components outside the range $|f| \le 1/T$;

(iv) $u(t)$ has negligible components outside the range $|f| \le 2/T$.

Next, we concentrate on the integral (34) and we maintain that, for $K>>1$, the following approximation holds true

$$\int_0^{KT} u(t)dt \cong \frac{T}{2}\sum_{k=1}^{2K} u\left(t_0 + \frac{kT}{2}\right), \tag{38}$$

where the sampling phase, t_0, is arbitrarily chosen in the interval $0 \le t_0 \le T/2$. Equation (38) is proved as follows. First, let us define

$$\bar{u}(t) \triangleq \begin{cases} u(t) & 0 \le t \le KT \\ 0 & \text{else} \end{cases} \tag{39}$$

and call $\bar{U}(f)$ the Fourier transform of $\bar{u}(t)$. Clearly, if K is large, the components of $\bar{u}(t)$ are confined in the same interval as those of $u(t)$. In other words

$$\bar{U}(f) \cong 0 \quad \text{for} \quad |f| \ge 2/T. \tag{40}$$

Second, application of Poisson sum formula [21, p.72] yields

$$\frac{T}{2}\sum_{k=1}^{2K} \bar{u}\left(t_0 + \frac{kT}{2}\right) = \sum_{k=-\infty}^{\infty} \bar{U}\left(\frac{2k}{T}\right)e^{i4\pi k t_0/T}, \tag{41}$$

or, because of (40),

$$\frac{T}{2}\sum_{k=1}^{2K} \bar{u}\left(t_0 + \frac{kT}{2}\right) = \bar{U}(0). \tag{42}$$

Third, since the integral of $u(t)$ over $0 \le t \le KT$ equals the integral of $\bar{u}(t)$ over the entire line, one has

$$\int_0^{KT} u(t)\,dt = \bar{U}(0), \tag{43}$$

so that, comparing with (42), one concludes that

$$\int_0^{KT} u(t)dt = \frac{T}{2}\sum_{k=-\infty}^{\infty} \bar{u}\left(t_0 + \frac{kT}{2}\right). \tag{44}$$

At this point (38) follows from (44), bearing in mind the definition of $\bar{v}(t)$ in (39).

Returning to (34) and making use of (35) and (38) we have

$$\frac{\partial \Lambda(\tilde{\nu})}{\partial \tilde{\nu}} = T\sum_{k=1}^{2K}\sum_{m=0}^{M-1} \mathrm{Im}\left\{x_m\left(\frac{kT}{2} + t_0\right)y_m^*\left(\frac{kT}{2} + t_0\right)\right\}. \tag{45}$$

We look for that value of $\tilde{\nu}$, say $\hat{\nu}$, where the right hand side of this equation vanishes. This problem may be solved by resorting to the recursion:

$$\hat{\nu}(k+1) = \hat{\nu}(k) + \gamma e_k, \tag{46}$$

where $\hat{\nu}(k)$ is the k-th estimate of ν, $e(k)$ is the k-th term in (45) and γ is a parameter (step size). In the following we adopt this method with two minor changes. First, we collect into $e(k)$ both the k-th and the $(k+1)$-th term. In this way $\hat{\nu}(k)$ can be updated every T seconds instead of $T/2$. Second, to keep the computing load as small as possible, we replace the integer M in the internal summation by $M' \le M$. In summary, we write

$$e(k) = \Gamma\sum_{m=0}^{M'-1} \mathrm{Im}\left\{x_m(t_{k-1/2})\,y_m^*(t_{k-1/2}) + x_m(t_k)\,y_m^*(t_k)\right\}, \tag{47}$$

where Γ is an arbitrary constant and the instants t_k and $t_{k-1/2}$ are defined as $t_k \triangleq kT + t_0$, $t_{k-1/2} \triangleq kT - T/2 + t_0$. For convenience, we choose $\Gamma \triangleq E_b T^2/4$. As we shall see in the next section, this makes the average of $e(k)$ independent of the signal power.

Figure 1 shows a block diagram for the carrier frequency estimator discussed above. The part enclosed in dashed lines represents the FDD. It is formed by pairs of matched filters, $h_m(-t)$ and $h'_m(-t)$, which provide $x_m(t)$ and $y_m(t)$. The loop filter performs the recursion (46) and the voltage controlled oscillator (VCO) generates the exponential $e^{-j\varphi(t)}$, with

$$\frac{d\varphi(t)}{dt} = 2\pi\hat{\nu}(k) \quad \text{for} \quad kT + t_0 \le t \le (k+1)T + t_0. \tag{48}$$

Several issues regarding this scheme come to mind. One is about implementation complexity: since the number of Laurent components may be large (with partial response systems), so might be the number of matched filter pairs required in Fig. 1. One wonders how many pairs are really needed in practice. Another issue is the loop performance: how can it be assessed and how is it affected by reducing the number of matched filters? These questions are addressed in the next section. For space limitations we skip the details and concentrate only on the final results. Methods to approach these problems are well known in the literature [11]-[13].

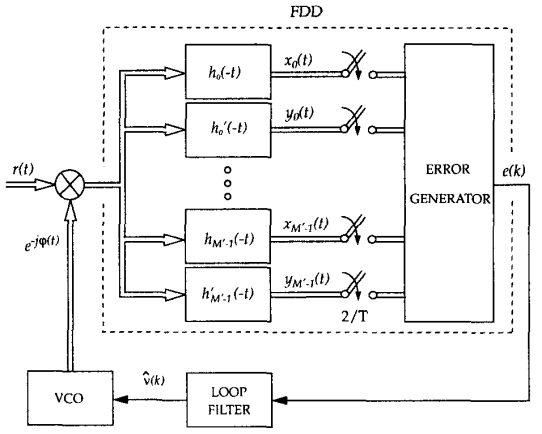

Fig.1. Block diagram of the carrier frequency loop.

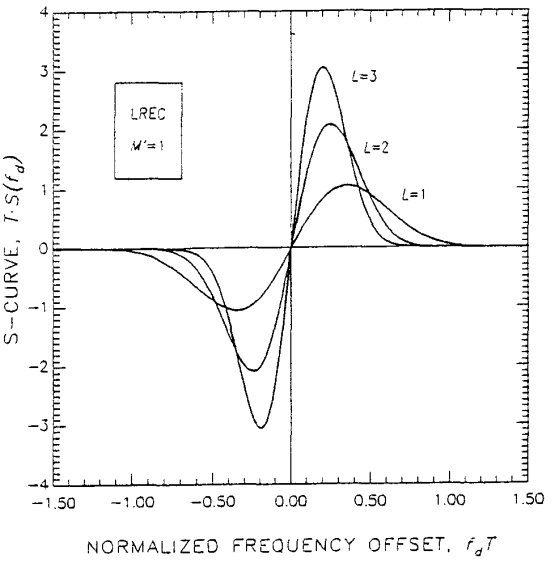

Fig.2. S-curves for LREC format.

VI. S-Curves and Tracking Errors

A. S-Curve.

The S-curve of the FDD is a key characteristic that establishes the loop acquisition properties. It is defined as the expectation of $e(k)$ (over data and thermal noise), conditioned on a fixed value of the difference, $f_d \triangleq \nu - \hat{\nu}$, between carrier frequency offset and its estimate. The S-curve is denoted $S(f_d)$.

Its calculation is straightforward and the result is:

$$S(f_d) = \frac{1}{2} \sum_{m=0}^{M'-1} \sum_{\ell=0}^{M'-1} \sum_{i=-\infty}^{\infty} \mathrm{Im}\left\{ g_{\ell,m}(\bar{t}_{i-1/2}, f_d) g'^{*}_{\ell,m}(\bar{t}_{i-1/2}, f_d) + g_{\ell,m}(\bar{t}_{i-1/2}, f_d) g'^{*}_{\ell,m}(\bar{t}_{i-1/2}, f_d) \right\}, \quad (49)$$

with $\bar{t}_i \triangleq iT + \Delta T$, $\bar{t}_{i-1/2} \triangleq iT - T/2 + \Delta T$, $\Delta T \triangleq t_0 - \tau$. The functions $g_{\ell,m}(t, f_d)$ and $g'_{\ell,m}(t, f_d)$ are defined as

$$g_{\ell,m}(t, f_d) \triangleq \frac{1}{T}\left[h_\ell(t) e^{j2\pi f_d t} \right] \otimes h_m(-t) \quad (50)$$

$$g'_{\ell,m}(t, f_d) \triangleq \frac{1}{T^2}\left[h_\ell(t) e^{j2\pi f_d t} \right] \otimes h'_m(-t), \quad (51)$$

where $\otimes$ is the convolution operation.

The following remarks are of interest:

- Formally, $S(f_d)$ depends on Δt, the difference between the sampling phase t_0 and the channel delay τ. As we have seen in the previous section, however, the error $e(k)$ is almost independent of t_0 and, therefore, we expect that the same holds true with $S(f_d)$. Numerical results confirm this fact. In consequence, the sampling operations in Fig. 1 need not be locked to the incoming data stream. This is very convenient during frequency acquisition when no timing information is available at the receiver.
- With full response systems (L=1) one has M=M'=1 and (49) involves only one summation. With partial response systems, instead, M is greater than unity and $S(f_d)$ depends on the choice of M', the number of matched filter pairs in the frequency detector. Numerical results shown later indicate that the S-curves are approximately the same for $M' \geq 1$. In other words, the loop acquisition capability is not impaired if only a pair of matched filters is used.
- Summation over index i in (49) seems to involve many terms. Actually, $h_m(t)$ and $h'_m(t)$ are very short functions of time so that there are only few non-zero terms to take account of.
- From (49) it is seen that the shape of $S(f_d)$ is not affected by thermal noise. This same result has been found with other FDDs [11]-[13].

Figure 2 illustrates S-curves for LREC pulses. For any L, only one pair of matched filters (M'=1) is used. It is seen that the width of the S-curves decreases as L increases. This is intuitively clear since, increasing L reduces the signal bandwidth [17, chapter 4] and, correspondingly, the interval where the likelihood function (29) assumes significant values (bear in mind that the S-curve is the derivative of the average likelihood function).

Figure 3 shows similar results for LRC, while Fig. 4 corresponds to GMSK (with BT=0.25, see (9)). Finally, Fig. 5 gives an idea of the influence of M'. It appears that increasing the number of matched filters from two to four is immaterial for 3REC. This same conclusion holds true also in the other cases we have explored.

B Steady-State Frequency Errors.

Assume that the loop is in tracking mode and define $f_d(k) \triangleq \nu - \hat{\nu}(k)$ as the frequency error at t=kT. This error undergoes fluctuations about zero as a consequence of thermal noise and the random nature of the data. A significant measure of the loop tracking capability is the variance of $f_d(k)$, which can be computed through the following steps (see [22]):

(i) The slope, A, of the S-curve at the origin is calculated

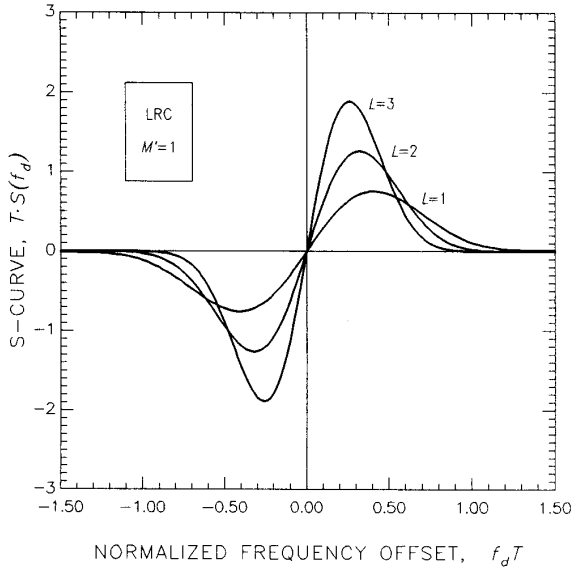

Fig.3. S-curves for LRC format.

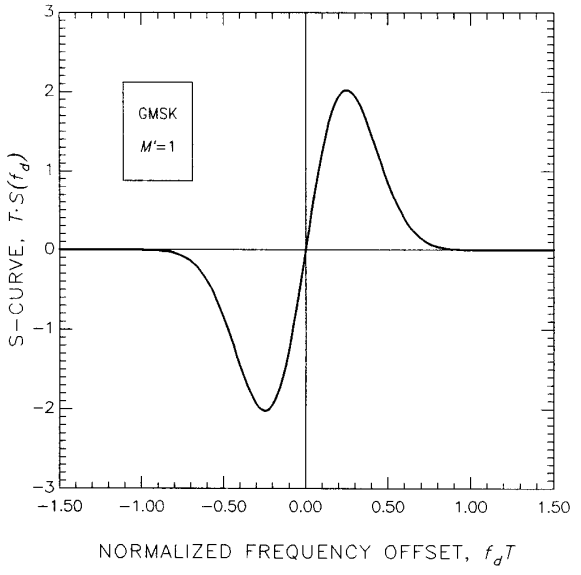

Fig.4. S-curves for GMSK.

from (49).

(ii) The autocorrelation of $e(k)/A$ is derived making use of (47).

(iii) The power spectral density of $e(k)/A$, $\mathcal{S}(f)$, is then computed by Fourier transformation.

(iv) Finally, the variance of $f_d(k)$ is obtained as:

$$\mathrm{Var}\{f_d(k)\} = \int_{-1/2T}^{1/2T} \mathcal{S}(f)\left|H\left(e^{j2\pi fT}\right)\right|^2 df, \qquad (52)$$

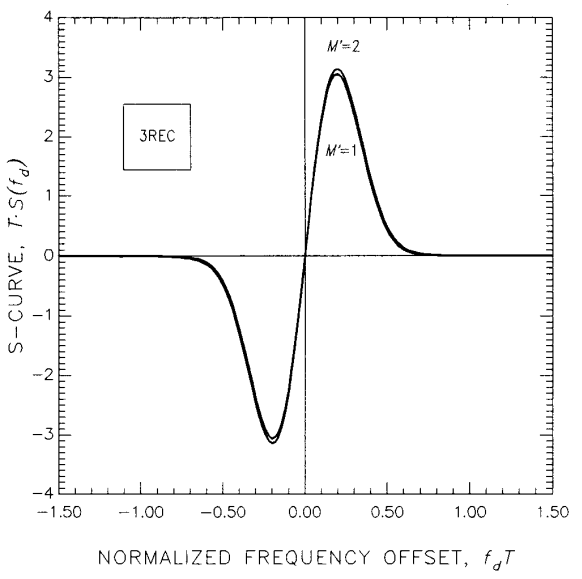

Fig.5. Illustrating the influence of M', the number of filter pairs.

where $H(z)$ is the loop transfer function

$$H(z) \triangleq \frac{\gamma A}{z-(1-\gamma A)}. \qquad (53)$$

Equation (52) can be simplified if $\mathcal{S}(f)$ is nearly constant in the frequency range where $H\left(e^{j2\pi fT}\right)$ assumes significant values. In this case $\mathrm{Var}\{f_d(k)\}$ depends only on $\mathcal{S}(0)$ and the one-sided noise equivalent bandwidth of the loop:

$$B_{EQ} \triangleq \frac{\gamma A}{2T(2-\gamma A)}. \qquad (54)$$

In other terms, letting $\sigma^2 \triangleq T^2\mathrm{Var}\{f_d(k)\}$, equation (52) becomes

$$\sigma^2 \equiv C \cdot B_{EQ}T, \qquad (55)$$

where C is a coefficient that depends on: (i) the CPM scheme; (ii) the signal-to-noise ratio, E_b/N_0; (iii) other parameters as, for example, the timing offset $\Delta t/T$ and the number of filter pairs in the frequency detector.

The following remarks about the computation of σ^2 are in order.

- We have found that the substitution $\mathcal{S}(f) \cong \mathcal{S}(0)$ in (52) is adequate for CPM schemes defined in (6)-(8), provided that B_{EQ} is sufficiently small. For example, Fig. 6 illustrates the shape of $\mathcal{S}(f)$ for 1REC and some values of the ratio $\Delta t/T$. It appears that all the curves have a flat region about the origin where they virtually coincide. Thus, for $B_{EQ}T \ll 1$, we expect that (55) gives accurate results and the coefficient C is almost independent of the timing offset $\Delta t/T$.

  To check this conclusion let us compare σ^2 as obtained from (52) (exact value) with that derived from (55) (approximate value). For $B_{EQ}T=10^{-2}$, $E_b/N_0=10$ dB and $\Delta t/T=0$ it is found that the former equals $3.63\cdot10^{-3}$ while

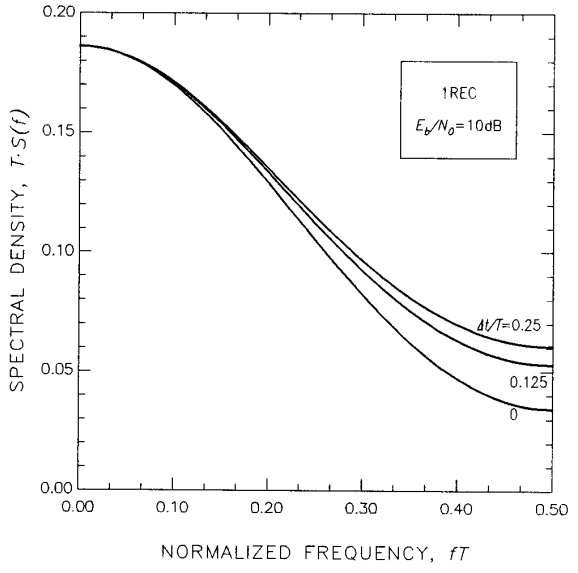

Fig.6. Shape of $S(f)$ for 1REC and some values of $\Delta t/T$.

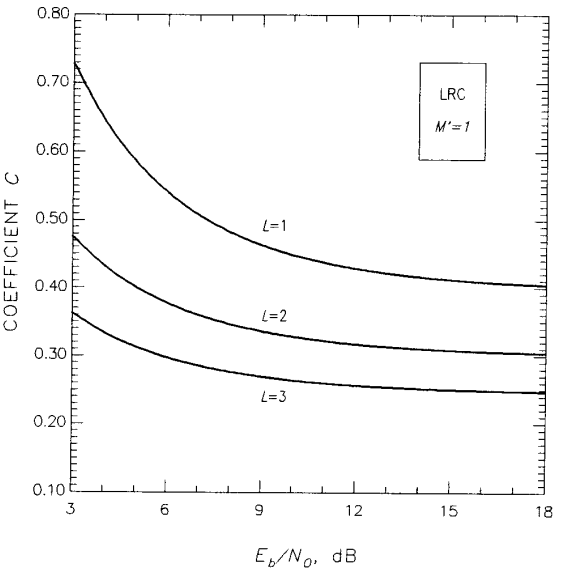

Fig.8. Coefficient C versus E_b/N_0 for LRC.

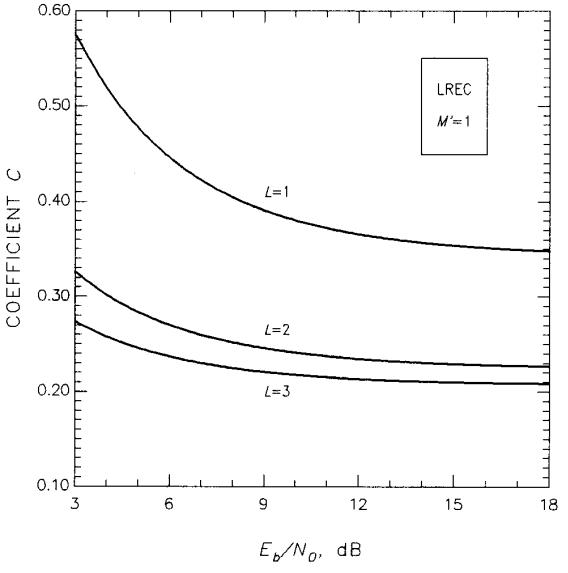

Fig.7. Coefficient C versus E_b/N_0 for LREC.

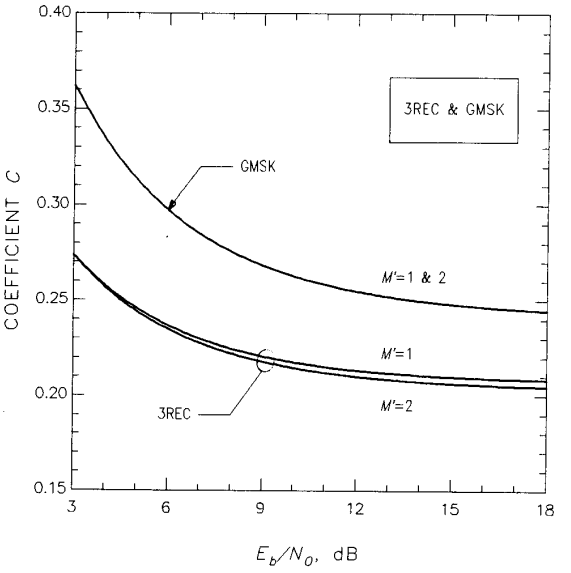

Fig.9. Illustrating the dependence of C on the number of filter pairs.

the latter equals $3.70 \cdot 10^{-3}$. Similarly, under the same conditions but with $\Delta t/T=0.25$, the exact value is still $3.63 \cdot 10^{-3}$ while the approximate value is $3.69 \cdot 10^{-3}$.

- The difficulties encountered in computing C depend on the CPM scheme. For full response systems ($L=1$) the calculation is straightforward (even if the final formula is messy). With partial response schemes, instead, the analytical approach is cumbersome and simulations seem the only viable route (for a given $B_{EQ}T$ one measures σ^2 and then derives C from (55)).
- Figures 7 and 8 show C versus E_b/N_0 for LREC and LRC schemes. The upper curve in each figure is obtained analytically while the others come from simulations (see next section). For any L only two pairs of filters ($M'=1$) are used in the frequency detector. It is seen that the tracking performance improves as L increases.
- The dependence of C on the number of filter pairs in the frequency detector is illustrated in Fig. 9. It appears that the dependence is weak, in general, and that there is no point in using more than a pair of filters.

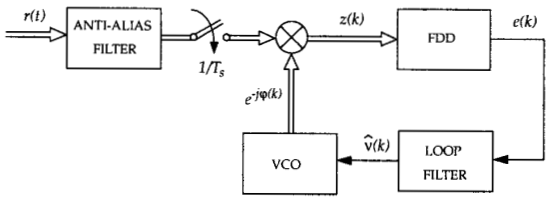

Fig.10. Digital implementation of the frequency recovery loop.

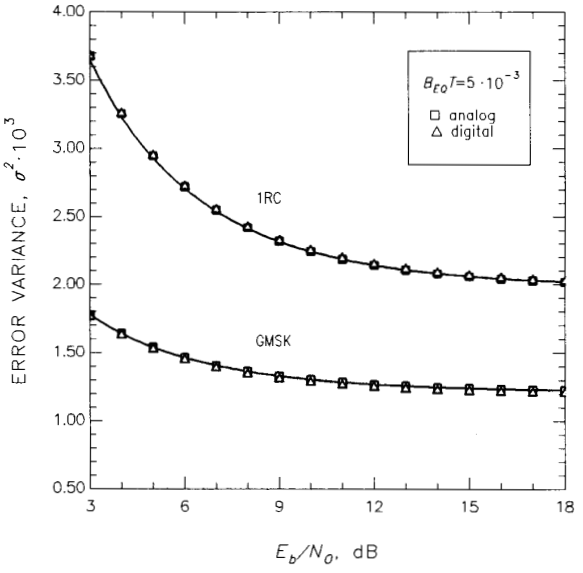

Fig.11. Loop tracking performance.

VII. SIMULATIONS

A. Digital implementation of the AFC loop.

So far the loop has been described as a hybrid system (VCO and FDD are analog while the loop filter is digital). We now consider its digital implementation, in the form illustrated in Fig. 10. The received waveform is first passed through an anti-alias filter and then is sampled at a rate $1/T_s=N/T$. Following the conclusions of the previous section, only a pair of matched filters is used. They are implemented as FIR structures whose tap coefficients are samples of the analog filter responses. They operate at rate N/T (but their outputs are decimated to $2/T$) and yield essentially the same outputs of their analog counterparts.

The loop filter operates as indicated in (46) and, accordingly, the estimates $\hat{v}(k)$ are updated at the symbol rate. The phase of the VCO, instead, is updated at the sampling rate and, in particular, its value increases by $2\pi\hat{v}(k)T_s$ at every step.

Key parameters are the bandwidth B_A of the anti-alias filter and the oversampling ratio $N=T/T_s$. A requirement of B_A is that it must be large enough to pass the signal components

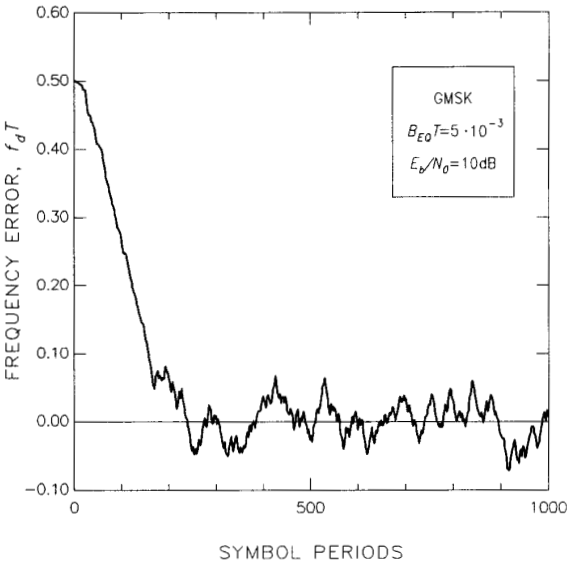

Fig.12. Loop acquisition for GMSK.

undistorted even when the carrier frequency offset v is at its maximum. Assuming a maximum equal to $1/T$, a conservative choice seems to be $B_A=2/T$ and $N=4$.

Loop tracking performance corresponding to these parameters has been investigated by simulation and is reported in Fig. 11 for 1RC and GMSK. In both cases a zero frequency offset is assumed ($v=0$). The anti-alias filter is an eight-pole Butterworth with equalized group-delay. Since no timing information is assumed, the sampling rate is taken as slightly different from the nominal value $4/T$ (actually, 1% lower). For comparison, the performance of the analog system is also shown (the corresponding simulations have been run with $B_A=6/T$ and $N=12$). The solid curve for 1RC has been computed from (55), using the coefficient C as given in Fig.8, while the curve for GMSK is just a graphycal interpolation of the simulation points.

It is interesting to compare these results with the performance limit expressed by the modified Cramer-Rao bound [23]

$$\mathrm{Var}\{f_dT\} \geq \frac{12\left(B_{EQ}T\right)^3}{\pi^2}\frac{1}{E_b/N_0}. \qquad (56)$$

For example, for $B_{EQ}T=5\cdot10^{-3}$ and $E_b/N_0=10$ dB, the right-hand side of (56) equals $1.52\cdot10^{-8}$ while, from Fig. 11, we read $\sigma^2=1.3\cdot10^{-3}$ for GMSK and $2.2\cdot10^{-3}$ for 1RC. It appears that the loop performance is far from the bound. This conclusion also applies to other frequency recovery schemes operating with no data information [8]-[13]. In fact, the major features of these schemes seem to be a comparatively large acquisition range and a relatively modest tracking performance.

Figure 12 illustrates loop acquisition with GMSK, from an initial frequency offset $v=0.5/T$. The acquisition time is about 200 symbol periods, i.e., on the order of $1/B_{EQ}T$.

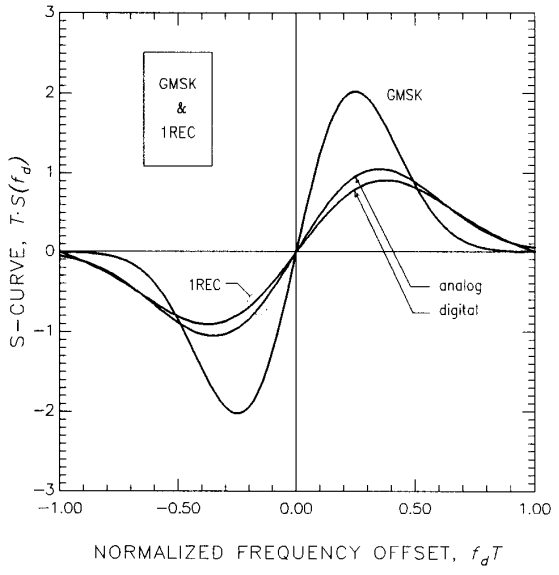

Fig.13. S-curves for 1REC and GMSK.

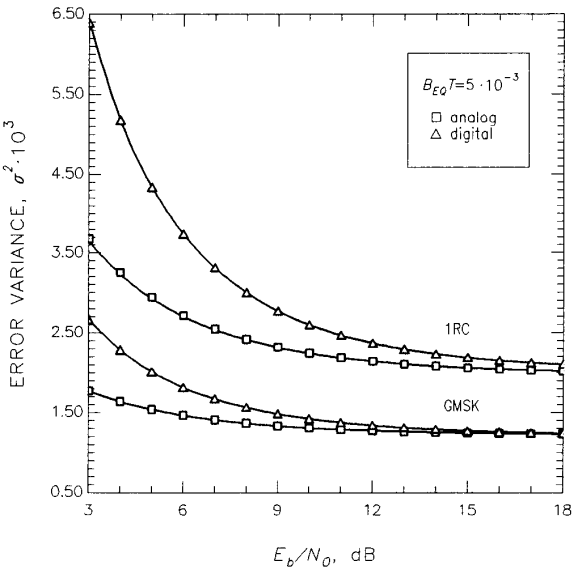

Fig.14. Error variance curves showing performance loss due to undersampling.

B. Reduced-complexity implementation.

The computational load associated with FDD filters can be halved by reducing the sampling rate from $4/T$ to $2/T$ (see also [12]). Results for this simplified implementation are reported in Figs. 13-14. The anti-alias filter bandwidth is still $B_A=2/T$.

Figure 13 illustrates S-curves for 1REC and GMSK. The curve for the 1REC analog detector is also shown for comparison (the one corresponding to GMSK coincides with its "digital" counterpart). It should be noted that S-curves for $2/T$ are obtained by simulation whereas those for $4/T$ are computed from (49). It is seen that sampling rate reduction has only a minimal effect.

Figure 14 gives error variance curves for 1RC and GMSK, assuming $\nu=0$. Performance losses due to undersampling are now visible, particularly at low E_b/N_0 values. Indeed, a 3 dB degradation in SNR occurs as a consequence of noise spectrum aliasing. Other error variance curves (not shown) indicate that these same conclusions are valid for ν-values in the range $\pm 1/T$.

VIII. Conclusions

New frequency detectors for binary CPM modulation formats have been proposed. They have been derived through ML methods and by exploiting Laurent's decomposition of CPM signals as sums of PAM waveforms. In this light, carrier frequency estimation for CPM appears as a generalization of the analogous problem for PAM signaling. Thus, it is not surprising that the solution we have found here is a generalization of that discovered in [11] in so far as, instead of a single pair of matched filters in the FDD, we now have several pairs. In most practical cases only one pair is important and the FDD scheme reduces to the one for PAM schemes.

Performance has been investigated in terms of acquisition capability and tracking errors. Analytical methods have been used in the case of full-response schemes, while a blend of analysis and simulation has been adopted with partial response signals. Acquisition range and tracking capability of the proposed algorithms are comparable with those of the frequency detectors discussed in [11].

Implementation issues have also been addressed. It has been pointed out that two samples per symbol are sufficient to implement frequency control loops endowed with a ML-based FDD.

References

[1] H.Sari and S.Moridi, "New Phase and Frequency Detectors for Carrier Recovery in PSK and QAM Systems", IEEE Trans. Commun., Vol. COM-36, pp. 1035-1043, Sept. 1988.

[2] J.C.-I. Chuang and N.R.Sollenberger, "Burst Coherent Demodulation with Combined Symbol Timing, Frequency Offset Estimation, and Diversity Selection", IEEE Trans. Commun., Vol. COM-39, pp.1157-1164, July 1991.

[3] M.P.Fitz, "Planar Filtered Techniques for Burst Mode Carrier Synchronization", GLOBECOM'91 Conf. Rec., Vol. I, pp. 365-369, Dec. 2-5, Phoenix, Arizona.

[4] C.R.Cahn, "Improving Frequency Acquisition of a Costas Loop", IEEE Trans. Commun., Vol. COM-25, pp. 1453-1459, Dec. 1977.

[5] F.D.Natali, "AFC Tracking Algorithms", IEEE Trans. Commun., Vol. COM-32, pp. 935-947, Aug. 1984.

[6] F.M.Gardner, "Properties of Frequency Difference Detectors", IEEE Trans. Commun., Vol. COM-33, pp. 131-138, Feb. 1985.

[7] F.M.Gardner, "Demodulator Reference Recovery Techniques Suited for Digital Implementation", ESA Final Report, ESTEC contract No 6847/86/NL/DG, Aug. 1988.

[8] A.N.D'Andrea, U.Mengali, "Performance of a Quadricorrelator Driven by Modulated Signals", IEEE Trans. Commun., Vol. COM 38, Nov. 1990.

[9] A.N.D'Andrea, U.Mengali, "Design of Quadricorrelators for Automatic Control System", IEEE Trans. Commun., June 1993, pp.988-997.

[10] T.Alberty and V.Hespelt, "A New Pattern Jitter Free Frequency Error Detector", IEEE Trans. Commun., Vol. COM-37, pp. 159-163, Feb.

1989.
[11] F.M.Gardner, "Frequency Detectors for Digital Demodulators Via Maximum Likelihood Derivation", ESA Final Report: Part II, ESTEC contract No 8022/88/NL/DG, March 1990.
[12] G.Karam, F.Daffara and H.Sari, "Simplified Version of the Maximum-Likelihood Frequency Detector", GLOBECOM'92 Conf. Rec.. Vol. 1, pp. 345-349, Dec. 1992, Orlando, FL.
[13] A.N.D'Andrea, U.Mengali, "Noise Performance of Two Frequency-Error Detectors Derived from Maximum Likelihood Estimation Methods", to appear in the April 1994 issue of the IEEE Trans. Commun.
[14] M.Luise and R.Reggiannini, "An Efficient Carrier Frequency Recovery Scheme for GSM Receivers", GLOBECOM'92 Conf. Rec. Commun. Theory Mini-Conf. Volume, pp.36-40, Dec. 6-9, Orlando, Florida.
[15] R.Melhan, Y.-E. Chen and H.Meyr, "A fully Digital Feedforward MSK Demodulator with Joint Frequency Offset and Symbol Timing Estimation for Burst Mode Mobile Radio", to appear in the IEEE Trans. on Vehicular Technology.
[16] P.A.Laurent, "Exact and Approximate Construction of Digital Phase Modulations by superposition of Amplitude Modulated Pulses", IEEE Trans. Commun., Vol. COM-34, pp. 150-160, 1986.
[17] J.B.Anderson, T.Aulin and C.-E.Sundberg, *Digital Phase Modulation*, New York: Plenum, 1986.
[18] G.Kawas Kaleh, "Simple Coherent Receivers for Partial Response Continuous Phase Modulation", IEEE J. Selec. Areas Commun. Vol. 9, pp.1427-1436, Dec. 1989.
[19] G.Kawas Kaleh, "Differential Detection Via the Viterbi Algorithm for Offset Modulation and MSK-Type Signals", IEEE Trans. on Vehicular Tech., Vol. 41, pp.401-406, Nov. 1992.
[20] H. L. Van Trees, *Detection, Estimation and Modulation Theory*. New York: Wiley, 1968.
[21] L.E.Franks, *Signal Theory*, Prentice-Hall, Englehood Cliffs, NJ, 1969.
[22] U.Mengali, "Joint Phase and Timing Acquisition in Data-Transmission", IEEE Trans. Commun. vol. COM-25, pp. 1174-1185, Oct. 1977.
[23] A.N.D'Andrea, U.Mengali and R.Reggiannini, "The Modified Cramer-Rao Bound and Its Application to Synchronization Problems", IEEE Trans. Commun., Vol. 42, No 2/3/4, pp.1391-1399, Feb./March/April 1994.

Aldo N. D'Andrea (M'82–SM'91) received the Dr.Ing. degree in electronic engineering from the University of Pisa, Italy, in 1977. From 1977 to 1981 he was a Research fellow engaged in research on digital phase-locked loops at the Centro Studi per i Metodi e i Dispositivi di Radiotrasmissione of the Consiglio Nazionale delle Ricerche (CNR). Since 1978 he has been involved in the development of the Italian Air Traffic Control Program (ATC). Currently, he is a Full Professor of Communication Systems at the Dipartimento di Ingegneria della Informazione, Università di Pisa. His interests include the design and analysis of digital communication systems, signal processing and synchronization.

Alberto Ginesi was born in Parma, Italy, 1967. He received the Laurea (cum Laude) in Electronic Engineering from the University of Pisa, in November 1993. Currently, he is involved in a Ph.D. program at the University of Pisa. His interests are in digital communication theory, with particular emphasis on synchronization algorithms.

Umberto Mengali (M'69–SM'85–F'90) received the Dr. Ing. Degree in Electrical Engineering from the University of Pisa in 1961 and the "Libera Docenza" in Telecommunications from the Italian Education Ministry in 1971. Since 1963 he has been with the Department of Information Engineering of the University of Pisa where he is a Professor of Telecommunications. His research interests are in digital communication theory, with emphasis on synchronization methods and modulation techniques. Professor Mengali is a member of the Communication Theory Committee and a former Editor of the IEEE Transactions on Communications (1985-1991). He is a Fellow of IEEE and is listed in American Men and Women in Science.